J Appl Electrochem (2013) 43:433–440
DOI 10.1007/s10800-013-0528-3

ORIGINAL PAPER

Study of the photo-electrochemical activity of cobalt- and nickel-doped TiO_2 photo-anodes for the treatment of a dye-contaminated aqueous solution

K. Esquivel · Ma. G. García · Francisco J. Rodríguez · Luis A. Ortiz-Frade · Luis A. Godínez

Received: 2 November 2012 / Accepted: 9 January 2013 / Published online: 26 January 2013

Abstract The photo-electrochemical activity of Co- and Ni-doped TiO_2 electrodes was studied using an aqueous solution containing an organic dye (Orange II) as a model polluted effluent. The results showed not only that both dopant species increased the activity of the photo-anode toward the dye color degradation but also that a specific proportion of the dopant materials maximized this effect. Interestingly, the best performance in the photo-electrochemical dye degradation process for the two doped materials was obtained using a 20 wt% doping synthetic proportion; achieving in both cases close to 90 % color removal during the first 10 min of reaction time. Employing the Langmuir–Hinshelwood formalism, the dopant effect was measured in terms of an increase in the kinetic rate coefficient and a coupled decrease in the dye adsorption equilibrium constant. In this way, while the surface rate constant (k_c) for the doped materials were found to be 3.3 (Co) and 2.7 (Ni) times higher than that of the un-doped TiO_2, the L–H adsorption constant were calculated as 0.083, 0.021, and 0.036 $(mgL^{-1})^{-1}$ for the TiO_2, Co- and Ni-doped materials, respectively. The results from additional experiments that followed the temporal evolution of the concentration of electro-generated H_2O_2 suggested a Fenton-like effect with regard to the anode performance caused by the doping species in the semiconductor anode.

Keywords Ni · Co · TiO_2 photo-anode · Electro-generated H_2O_2 · Photo-electrocatalysis

K. Esquivel · F. J. Rodríguez · L. A. Ortiz-Frade · L. A. Godínez (✉)
Centro de Investigación y Desarrollo Tecnológico en Electroquímica, S. C., Parque Tecnológico Querétaro–Sanfandila, P.O. Box 064, C.P. 76703 Pedro Escobedo, Qro, Mexico
e-mail: lgodinez@cideteq.mx
URL: http://www.cideteq.mx

Present Address:
K. Esquivel
Universidad Autónoma de Querétaro, Cerro de las Campanas s/n, C.P. 76010 Santiago de Querétaro, Qro, Mexico

Ma. G. García
Universidad de Guanajuato, Calle Lascuraín de Retana, C.P. 36000 Guanajuato, Gto, Mexico

1 Introduction

Owing to their recalcitrant nature, water effluents contaminated with synthetic dyes cannot be effectively treated using conventional biologic processes and therefore are ideal candidates for advanced oxidation technologies [1, 2]. Advanced oxidation processes (AOPs) are characterized by the generation and use of the hydroxyl radical ($^{\bullet}OH$), a strong oxidant species that, under certain conditions, is capable of mineralizing a wide variety of organic contaminants [3, 4]. One of the most popular AOPs for the removal of persistent organic pollutants from water is based on the Fenton reaction [5]. Fenton's reagent consists of a mixture of H_2O_2 and Fe(II) ions that results in the generation of the $^{\cdot}OH$ species.

As will be discussed below, H_2O_2 can be produced through the electrochemical reduction of dissolved oxygen, resulting in electrochemical advanced oxidation processes (EAOPs) [6, 7]. EAOPs can also be photo-assisted through the use of illuminated semiconductor anodes in the electrochemical reactor, which contribute to the production of H_2O_2 from water oxidation in addition to the peroxide formed from oxygen reduction at the cathode [8, 9].

Therefore, the photo-assisted EAOPs result in photo-electrochemical advanced oxidation processes (PEAOPs) and several advantages can be envisioned when these systems are designed for wastewater treatment [10, 11]. The most attractive advantages include the environmental compatibility because the main reagent, the electron, is a clean reagent, and the operational simplicity, as the use of the semiconductor electrodes does not require separation processes to recover the catalyst as in the case of technologies that impose the need for filtration or centrifugation.

In the context of the design of PEAOP-based technologies, titanium dioxide (TiO_2) has been the most widely studied photo-anode material due to its non-toxicity, low cost, and long-term photo-stability. However, the photocatalytic efficiency of TiO_2 is limited by its large band gap (3.2 eV), which requires UV radiation to be activated [12]. As a result, TiO_2 absorbs only 3–5 % of the energy of the solar spectrum, and several studies have therefore been conducted to prepare TiO_2-based materials that can be activated using visible light [13–18]. One of these approaches involves substituting a fraction of the Ti atoms into the semiconductor lattice with transition metals via doping. In addition to reducing the band gap, doped metals incorporated within the TiO_2 lattice have been shown to promote other interesting effects with regard to the photocatalytic activity of the TiO_2 electrodes, such as decreasing the electron–hole recombination rate, changes in the surface charge carrier trap population, and changes in the kinetics of electron (e^-) or hole (h^+) transfer [15–18].

Within this context, the present study focuses on the effects of the incorporation of M (Co or Ni) into the TiO_2 lattice of nanoparticulated thin film-based anodes, which were used to perform the photo-electrochemical oxidation of a model pollutant in a synthetic aqueous effluent that also contained electro-generated H_2O_2 at the cathode. In contrast to the standard Fenton-based PEAOP in which Fe(II) ions are added to the working solution, the experiments described in this study were performed in the absence of dissolved Fe species to isolate the effect of the dopant atoms on both the electrochemical decomposition reaction of H_2O_2 at the anode and on the photo-catalytic activity of the doped TiO_2 electrodes used to oxidize the organic dye.

2 Materials and methods

2.1 Synthesis and characterization of nickel- and cobalt-doped TiO_2 films

Preparation of the M:TiO_2 materials, where M stands for either Co or Ni, was performed following a previously reported methodology with minor modifications [19, 20]. With this approach, several M:TiO_2 wt% ratios (from 5 to 50 %) were employed to prepare nanoparticles of the differently modified TiO_2 materials. Both cobalt (Caledon 98 % pure) and nickel (Alpha Aesar 99 % pure) were obtained as hydrated acetate salts. As previously reported, the M:TiO_2 films were prepared by the deposition of the relevant nanoparticulated semiconductor onto ITO glass substrates by the electrophoretic deposition method [20]. The characterization of these materials was conducted by SEM, EDS, Diffuse Reflectance, XRD, Rietvel Refinement, and Raman analysis and the corresponding results have already been reported [19].

2.2 Photo-electrochemical experiments

Photo-electrochemical experiments to assess the oxidation capacity of the anodic materials under study were performed using a glass cell containing a vitreous glassy carbon electrode as the cathode (2 cm^2 geometric area) and a TiO_2 or M:TiO_2 semiconductor electrode as the anode. As depicted in Fig. 1, the photo-electrochemical cell was fitted with a Hg/Hg_2SO_4 reference electrode, an O_2 bubbling system and a UV lamp (UVP pen ray lamp, $\lambda = 365$ nm, $P = 0.75$ μW cm^{-2}). The electrolytic solution consisted of a mixture of 0.05 M Na_2SO_4 (adjusted to pH 3 with H_2SO_4) and Orange II dye (Aldrich) at concentrations that ranged between 5 and 60 mg L^{-1}. As has been previously reported, oxygen saturation conditions were achieved by bubbling the electrolytic solution for 15 min with pure oxygen gas (99.9 %, Infra) before the experiment, and by maintaining the O_2 gas flow above the solution surface throughout the experiment [6, 7, 21].

As previously mentioned, H_2O_2 was electrochemically produced from the reduction of oxygen as described by Eq. 1.

$$O_{2(g)} + 2H^+ + 2e^- \rightarrow H_2O_2 \quad (1)$$

In order to promote the reaction described in this Eq., a −0.95 V potential difference between the carbon and the reference ($Hg/HgSO_4$) electrodes was applied using a Volta-Lab potentiostat/galvanostat (PGZ 301).

The oxidation of the Orange II dye species was related to the direct electrochemical reaction of the dye at the semiconductor surface and to its reaction with the $^{\bullet}OH$ radicals that were produced from the H_2O_2 electrochemical oxidation and the photo-induced decomposition. As has been previously reported, the oxidation of the dye molecule was followed by monitoring the spectrophotometric measurement changes of the azo bond maximum absorbance signal of the dye molecule at $\lambda = 487$ nm using a UV–Vis Agilent spectrophotometer [6, 11].

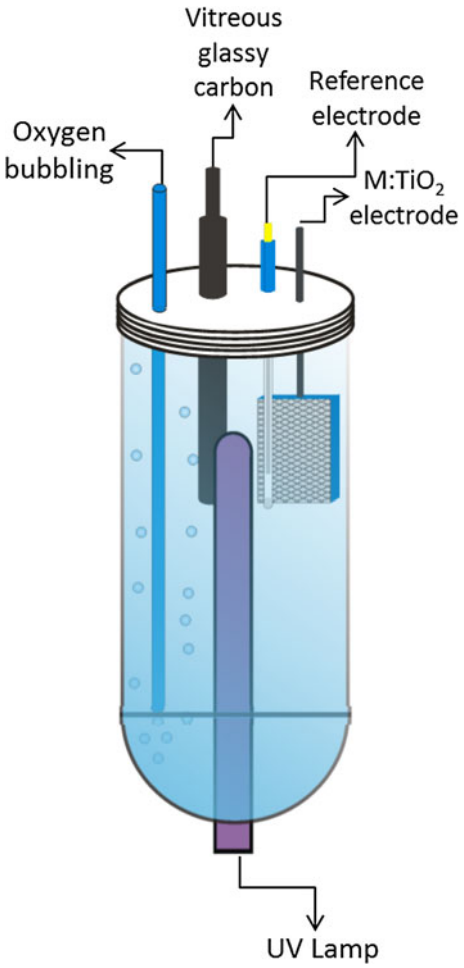

Fig. 1 Experimental setup for the photo-electro-catalytic experiments

2.3 Study of the decomposition of electro-generated H_2O_2 by undoped TiO_2 and doped (Co:TiO_2 and Ni:TiO_2) anodes

Using the PGZ 301Volta-Lab potentiostat, electrochemical tests were performed to gain insight on the role of the doping transition metals on the H_2O_2 decomposition reactions. To conduct the experiments, a piece of carbon cloth (WE, 0.2 cm^2 geometric area) was placed on one side of the UV–Vis cuvette and polarized at −0.75 V versus a Ag/AgCl reference electrode, and the TiO_2/ITO or M:TiO_2/ITO substrate (CE, 0.5-cm^2 geometric area) was positioned perpendicularly onto one of the transparent windows of the cuvette. The contents of the cuvette consisted of a previously O_2-saturated solution (see Sect. 2.2) maintained at a pH of 3 using a sodium sulfate buffer. For the control experiment in which the Fenton reagent was investigated, an Fe-loaded piece of Nafion membrane was placed in the reaction cell [21, 22]. The amounts of electro-generated H_2O_2 at the different reaction times were determined by spectrophotometric measurements (Ocean Optics spectrophotometer, USB4000, Toshiba detector TCD1304AP) by the titanium (IV) oxy-sulfate method ($TiOSO_4$, 99.99 %, ca. 15 wt% diluted sulfuric acid solution, Aldrich), which is based on the color intensity measurement of the Ti(IV)-H_2O_2 complex that absorbs at 406 nm [23]. Absorbance measurements were obtained every 30 s for 60 min.

3 Results and discussion

3.1 Photo-electrochemical oxidation of orange-II dye in aqueous solution

The results of the dye oxidation experiments performed using the Co:TiO_2 thin film anodes prepared at different Co doping ratios are shown in Fig. 2. Inspection of this figure reveals that the trend in absorbance decreases were similar between TiO_2 and the Co:TiO_2 materials. Although all the surveyed electrodes promoted the complete color disappearance of the dye after 60 min, it is interesting to note that the reduction rate of the initial absorbance was more pronounced for the doped anodes than for the control TiO_2 electrode. In this way, while the absorbance ratio of the dye decreased by 5 % when TiO_2 was used as an anode within the initial 5 min, the conversion of the organic dye reached 30 % when Co (5 wt%) was incorporated into the TiO_2 lattice of the semiconductor electrode. Better conversions were obtained by increasing the amount of Co atoms in the TiO_2 structure, reaching 65 % of Orange II decomposition when 20 wt% of Co was used. Interestingly, larger doping ratios resulted in lower initial dye conversion rates,

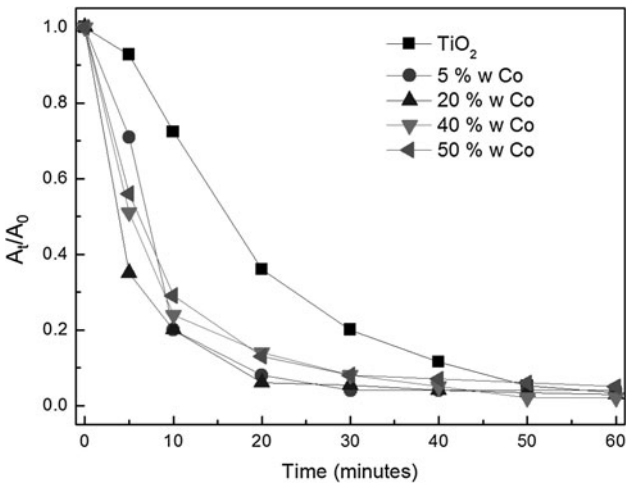

Fig. 2 Absorbance ratios (A/A_0) vs. time for different wt% doping of Co:TiO_2 electrodes. $[OG\ II]_0 = 50$ mg L^{-1}. Electrolyte: 0.05 M Na_2SO_4, pH 3. UV radiation: $\lambda = 365$ nm, $P = 0.75$ μW/cm^2. $E_{appl} = -0.95$ V vs. Hg/Hg_2SO_4

reaching approximately 45 % absorbance ratio values with the higher doping proportions (40 and 50 wt% of Co). These results indicate that the initial rate of the chemical reaction was clearly affected by the presence of the doping Co species and that this rate was maximized at a 20 wt% Co:TiO_2 doping ratio of the semiconductor anode material.

Similar behavior was obtained in the Orange II photoelectrochemical oxidation experiments using the Ni:TiO_2 electrodes (see Fig. 3). In this case, however, the initial rate of reduction of the absorbance ratio with 5 wt% of Ni reached 40 % within the initial 5 min of reaction, which was 10 % faster than the rate obtained for the same Co:TiO_2 ratio. Figure 3 also shows that after the first five minutes of the experiment, the dye conversion reached 60 % when 20 wt% of Ni was employed, which was only 5 % lower than the value measured for the corresponding Co:TiO_2 ratio. In spite of these differences, however, it is interesting to note that, as in the case of the Co-doped material, 20 wt% of Ni resulted in the greatest initial rate for the decrease in dye absorbance. In addition, larger proportions of doping agent in the anode resulted in slightly lower color disappearance ratios (approximately 50 % for both 40 and 50 wt% Ni-doped electrodes). Although the observed differences between the Co- and Ni-modified materials were not substantial, it is important to note that the effect of the two metal doping agents was significant when compared to the initial dye absorbance decrease rate of the un-doped TiO_2 electrode.

3.2 Kinetic analysis

Using the data shown in Figs. 2 and 3, dye concentration versus time plots were constructed for the complete experiments assuming a first-order reaction model (see Fig. 4a, b). Inspection of these plots reveals that a kinetic model in which the reaction rate depended only on the rate constant and on the concentration of the dye worked reasonably well as a first approximation.

As can be observed from the corresponding data presented in Table 1, all the rate constant values calculated for the doped semiconductor electrodes were larger than that of the TiO_2 substrate, and values between the Co- and Ni-doped substrates were similar between the corresponding metal dopant proportions. Furthermore, it is important to note that, using the complete time span of the experiment, the largest rate constants for the two doped materials corresponded to those prepared with 20 wt% doping agent.

Inspection of Fig. 4 also reveals that at $t = 0$, the intercept of the fitted lines do not converge to zero, suggesting that a different kinetic model was required to accurately reflect the kinetics of the dye decomposition.

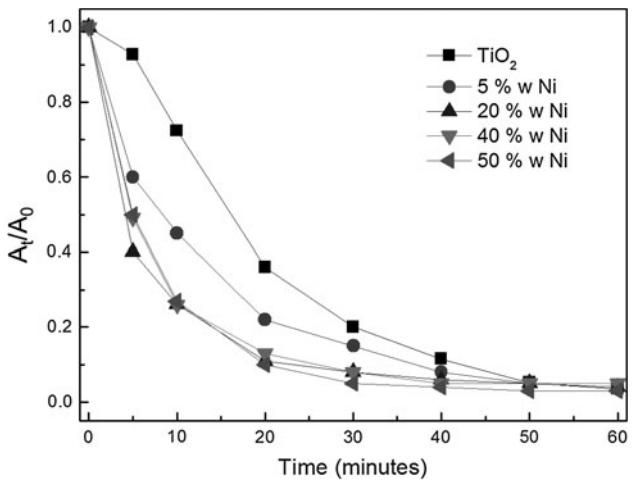

Fig. 3 Absorbance ratios (A/A_0) vs. time for different wt% doping of Ni:TiO_2 electrodes. $[OG\ II]_0 = 50$ mg l^{-1}. Electrolyte: 0.05 M Na_2SO_4, pH 3. UV radiation: $\lambda = 365$ nm, $P = 0.75$ μW/cm^2. $E_{appl} = -0.95$ V vs. Hg/Hg_2SO_4

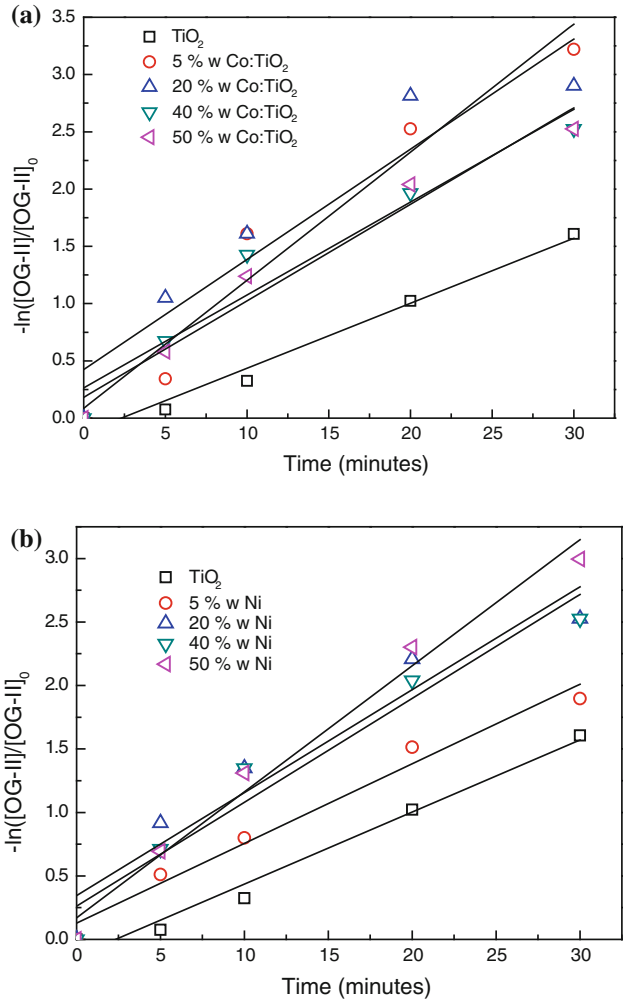

Fig. 4 Logarithmic plot of azo OG-II dye color removal using TiO_2 and different wt% doping ratios in **a** Co:TiO_2 and **b** Ni:TiO_2 electrodes. $[OG\ II]_0 = 50$ mg L^{-1}. UV radiation: $\lambda = 365$ nm, $P = 0.75$ μW/cm^2. $E_{appl} = -0.95$ V vs. Hg/Hg_2SO_4

Table 1 Rate constant values for the different modified materials (5, 20, 40, and 50 wt% of Co and Ni)

k (min^{-1})		R^2
Cobalt		
TiO_2	0.056	0.987
5 wt%	0.111	0.968
20 wt%	0.135	0.927
40 wt%	0.081	0.961
50 wt%	0.084	0.977
Nickel		
TiO_2	0.056	0.987
5 wt%	0.062	0.985
20 wt%	0.099	0.949
40 wt%	0.081	0.967
50 wt%	0.081	0.989

To verify this assumption, the effect of the initial concentration of Orange II on the reaction rate was evaluated by performing experiments with 20 wt% M:TiO_2 electrodes and different starting concentrations of the dye in the 5 to 60 mg L^{-1}range. The results of these experiments were processed as previously described, and the rate coefficients were estimated by regression analysis using a first-order kinetic model.

As can be seen from the data presented in Table 2, the estimated values of the rate coefficients decreased as the initial concentration of the dye increased, thus confirming that a simple first-order kinetic model was not appropriate and suggesting that a coupled adsorption process of the dye was most likely involved.

The Langmuir–Hinshelwood formalism was employed to test this hypothesis. As can be seen in Eq. 2, the rate, r, depends on the activity of the dye, $[OG_{II}]$, and on an experimental coefficient, k_{obs}, the inverse ($1/k_{obs}$) of which is a linear function (Eq. 3) of the initial activity of the dye, $[OG_{II}]_0$, the rate constant for its oxidation, k_c, and an adsorption equilibrium constant, $K_{OG_{II}}$, of the organic molecule on the surface of the anode in which the oxidation reaction takes place (TiO_2 or M:TiO_2).

$$r = k_c \frac{K_{OG_{II}}[OG_{II}]}{1 + K_{OG_{II}}[OG_{II}]_0} = k_{obs}[OG_{II}] \quad (2)$$

$$\frac{1}{k_{obs}} = \frac{1}{k_c K_{OG_{II}}} + \frac{[OG_{II}]_0}{k_c} \quad (3)$$

The assumption was made with this model that as the initial concentration of organic dye approaches zero, k_{obs} becomes $k_c K_{OG_{II}}$ (see Eq. 3), leading to the pseudo-first-order kinetics predicted by Eq. 2. Then, as the initial concentration of the organic dye increases, the value of k_{obs} should decrease, as predicted by Eq. 3 and reflected by the data shown in Table 2. The experimental data were therefore fitted to the Langmuir–Hinshelwood model (see Fig. 5) using the observed pseudo-first-order coefficients and the different initial concentrations of the dye. From the resulting fitted parameters shown in Table 3, the presence of the doping agent in the TiO_2 structure clearly enhanced the reaction rate, k_c, by a factor of nearly 3.3 for Co (10.526 mg L^{-1} min^{-1}) and 2.7 for Ni (8.475 mg L^{-1} min^{-1}) when compared to the unmodified TiO_2 semiconductor material (3.145 mg L^{-1} min^{-1}).

Inspection of the fitted adsorption equilibrium constants, $K_{OG_{II}}$, on the other hand, revealed that the doping resulted in lower values for the Co- (0.021 L mg^{-1}) and Ni-doped materials (0.036 L mg^{-1}) when compared to TiO_2 (0.083 L mg^{-1}). These parameters therefore suggested that the dye reacted quickly on the surface of the doped semiconductor materials, thus inhibiting the blocking of the active sites of the electrode surface, as occurs in the un-doped TiO_2 substrate [24].

3.3 Effect of the doping agent of the TiO_2 anodes on the balance of electro-generated H_2O_2

The results described above indicated that the presence of the doping agent in the TiO_2 anode not only increased the

Table 2 Rate constant values obtained using 20 wt% Co- and Ni-modified TiO_2 electrodes and different initial dye concentrations

Initial dye concentration (mg L^{-1})	k_{obs} (min^{-1})					
	TiO_2	R^2	$Co_{(20\ wt\%)}$: TiO_2	R^2	$Ni_{(20\ wt\%)}$: TiO_2	R^2
5	0.43479	0.989	0.51755	0.933	0.53529	0.979
10	0.14517	0.991	0.18564	0.948	0.24825	0.944
15	0.11436	0.966	0.13744	0.954	0.20259	0.955
25	0.0913	0.972	0.13717	0.997	0.13304	0.967
30	0.06778	0.961	0.12377	0.994	0.13268	0.997
40	0.06214	0.966	0.12504	0.977	0.12739	0.986
50	0.06051	0.959	0.10419	0.938	0.10425	0.992
60	0.05897	0.982	0.09655	0.947	0.10213	0.971

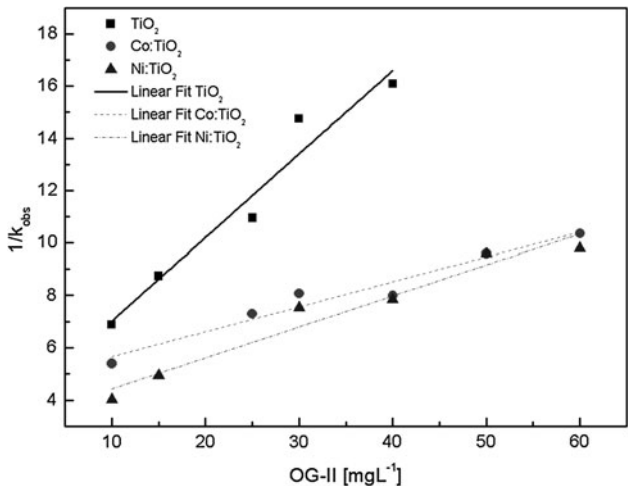

Fig. 5 Langmuir–Hinshelwood fitted lines for TiO_2 (*filled square*) and 20 wt% of Ni:TiO_2 (*filled trianlge*) and Co:TiO_2 (*filled circle*)

Table 3 Fitted rate and adsorption constant values of the Langmuir–Hinshelwood model for TiO_2 and 20 wt% of Ni:TiO_2 and 20 wt% Co:TiO_2

Electrode	k_c (mg $L^{-1}min^{-1}$)	K_{OGII} (mg $L^{-1})^{-1}$	R^2
TiO_2	3.145	0.083	0.968
20 wt% Co:TiO_2	10.526	0.021	0.972
20 wt% Ni:TiO_2	8.475	0.036	0.972

dye oxidation kinetics but also decreased the extent of adsorption of the organic molecule onto the electrode surface. This observation suggested the presence of an increased $^{\bullet}OH$ radical concentration at the semiconductor-electrolyte interface of the doped electrodes. As shown by Eq. 4, the illumination of any of the semiconductor electrodes under study (SE) resulted in the generation of a given amount of electron–hole pairs that were separated by the potential imposed to the cell.

$$SE + h\nu \rightarrow e^-_{cb}(external\ circuit) + h^+_{vb} \quad (4)$$

In addition to the direct photo-electrochemical oxidation of the dye, Eq. 5 and 6 describe how the photo-generated holes reacted with water and H_2O_2 molecules to produce the $^{\bullet}OH$ radicals, a species that, due to their oxidation power, could have been responsible for the changes in the kinetic and adsorption parameters that characterized the performances of the doped TiO_2 electrodes.

$$2H_2O + 2h^+_{vb} \rightarrow H_2O_2 + 2H^+ \quad (5)$$

$$h^+ + H_2O_2 \rightarrow {}^{\bullet}OH + {}^{-}OH \quad (6)$$

It is interesting to note that Eq. 6 resembles the well-known Fenton reaction (see Eq. 7, with M corresponding to Fe) that, in this case, could correspond to a Fenton-like reaction in which M would be the doping metal in the TiO_2 structure.

$$M^{2+} + H_2O_2 \rightarrow M^{3+} + {}^{\bullet}OH + {}^{-}OH \quad (7)$$

To explore if the doping metal could play a Fenton-like role in the modified electrodes under study, a series of experiments was performed in which the concentration of H_2O_2 was monitored by UV–Vis measurements. As described in the experimental section, spectro-electrochemical tests were performed in a previously oxygen-saturated solution to study the balance of the coupled cathodic generation and anodic decomposition of H_2O_2 as a function of time. The results of these experiments are shown in Fig. 6a, b, c for the TiO_2 electrode and the two modified anode composites.

A quick inspection of these curves reveals that, in all cases, there existed a period of time at the beginning of the experiment (region (I)) in which the progressive cathodic generation of H_2O_2 (see Eq. 1) explained the spectroscopic response. As dissolved, O_2 was depleted in the solution and the electrochemically produced H_2O_2 reached the semiconductor electrode, the anodic decomposition of the peroxide began to dominate (region II), reaching a spectroscopic response shape at longer times that reflected the depletion of peroxide (region III) due to Eq. 6 for the three anode materials and most likely Eq. 7 for the doped semiconductor electrodes.

Although the three regions were present in the H_2O_2 concentration versus time curves of Fig. 6a, b, c, it is important to note that the shapes of the spectroscopic responses of the two doped anode materials were substantially different than those of TiO_2, suggesting that the M-containing semiconductor electrodes were, as expected, more active toward H_2O_2 decomposition. To investigate the idea of a Fenton-like role of the doping species in the semiconductor electrode, a control experiment using an un-doped TiO_2 anode and Fe-loaded Nafion membrane immersed in the electrolytic solution was conducted [25–27]. As shown in Fig. 6d, the resulting spectroscopic response was clearly closer in shape to the curves obtained with the doped anodes than to the shape of the corresponding response of the experiment performed using the unmodified TiO_2 electrode. Although not conclusive, this observation supports the idea of a Fenton-like role of the doping metals in the semiconductor electrode.

4 Conclusions

In this work, we showed that the Co and Ni doping of TiO_2 anodes could enhance the rates of color removal of aqueous solutions of Orange II and that this effect was dependent on

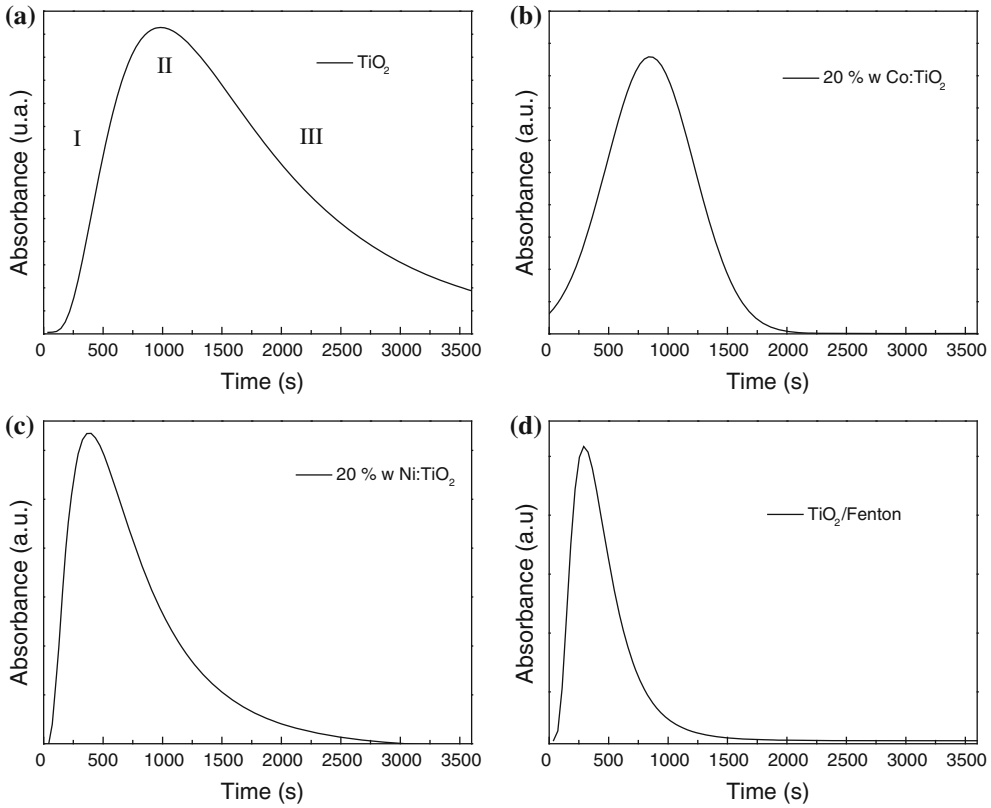

Fig. 6 Electro-generated H_2O_2 concentration vs. time profiles using **a** TiO_2, **b** 20 wt% Co:TiO_2, **c** 20 wt% Ni:TiO_2, and **d** TiO_2 and an Fe-modified Nafion membrane. Absorbance measurements were obtained at 406 nm. Electrolyte: 0.05 M Na_2SO_4. Carbon cloth as WE, TiO_2-, or TiO_2-modified materials as CE and Ag/AgCl as RE

the doping species concentration. Using the Langmuir–Hinshelwood formalism, we observed that, while 20 wt% M (Co or Ni) doping increased the rate of the reaction by a factor of approximately 3, the related dye adsorption constant decreased in a similar proportion. The faster oxidation kinetics observed for the doped materials were consistent with an inhibited dye adsorption process that eventually blocked the active sites of the oxidation reaction. Although spectro-electrochemical experiments also suggested that a Fenton-like process could characterize the anodic activity of the doped semiconductor anodes, further studies are necessary to fully investigate this hypothesis and to understand the effects of the doping agents on the electro- and photo-electrochemical properties of these modified materials.

Acknowledgments The authors thank the Mexican Council for Science and Technology (CONACyT, Grant SEP-CONACYT 167138, and Grant SEP-CONACyT CB-2008-106590) for financial support of this work. K.E.E. also acknowledges CONACyT for a graduate fellowship.

References

1. Han F, Kambala VSR, Srinivasan M, Rajarathnam D, Naidu R (2009) Tailored titanium dioxide photocatalysts for the degradation of organic dyes in wastewater treatment: a review. Appl Catal A 359:25–40
2. Martínez Huitle CA, Brillas E (2009) Decontamination of wastewaters containing synthetic organic dyes by electrochemical methods: a general review. Appl Catal B 87:105–145
3. Forgacs E, Cserhati T, Oros G (2004) Removal of synthetic dyes from wastewaters: a review. Environ Int 30:953–971
4. Gomathi DL, Girish KS, Mohan RK, Munikrishnappa C (2009) Photo degradation of methyl orange an azo dye by advanced Fenton process using zero valent metallic iron: influence of various reaction parameters and its degradation mechanism. J Hazard Mater 164:459–467
5. Özcan A, Oturan MA, Oturan N, Sahin Y (2009) Removal of acid orange 7 from water by electrochemically generated Fenton's reagent. J Hazard Mater 163:1213–1220
6. Peralta Hernández JM, Meas-Vong Y, Rodríguez FJ, Chapman TW, Maldonado MI, Godínez LA (2008) Comparison of hydrogen peroxide-based processes for treating dye-containing wastewater: decolorization and destruction of Orange II azo dye in dilute solution. Dyes Pigm 76:656–662
7. Peralta Hernández JM, Martínez Huitle CA, Guzmán Mar JL, Hernández Ramírez A (2009) Recent advances in the application of electro-Fenton and photoelectro-Fenton process for removal of synthetic dyes in wastewater treatment. Environ Eng Manag J 19:257–265
8. Lapertot M, Ebrahimi S, Oller I, Maldonado MI, Gernjak W, Malato S, Pulgarín C (2008) Evaluating Microtox© as a tool for biodegradability assessment of partially treated solutions of pesticides using Fe^{3+} and TiO_2 solar photo-assisted processes. Ecotox Environ Safe 69:546–555

9. Sun J, Qiao L, Sun S, Wang G (2008) Photocatalytic degradation of orange G on nitrogen-doped TiO_2 catalysts under visible light and sunlight irradiation. J Hazard Mater 155:312–319
10. Jain R, Sharma N, Radhapyari K (2009) Electrochemical treatment of pharmaceutical azo dye amaranth from waste water. J Appl Electrochem 39:577–582
11. Esquivel K, Arriaga LG, Rodríguez FJ, Martínez L, Godínez LA (2009) Development of a TiO_2 modified optical fiber electrode and its incorporation into a photoelectrochemical reactor for wastewater treatment. Water Res 43:3593–3603
12. Rauf MA, Ashraf SS (2009) Fundamental principles and application of heterogeneous photocatalytic degradation of dyes in solution. Chem Eng J 151:10–18
13. Kudo A, Niishiro R, Iwase A, Kato H (2007) Effects of doping of metal cations on morphology, activity, and visible light response of photocatalysts. Chem Phys 339:104–110
14. Kim DH, Choi DK, Kim SJ, Lee KS (2008) The effect of phase type on photocatalytic activity in transition metal doped TiO2 nanoparticles. Catal Commun 9:654–657
15. Martín C, Solana G, Malet P, Rives V (2003) Nb_2O_5-supported WO_3: a comparative study with WO_3/Al_2O_3. Catal Today 78: 365–376
16. Meng F, Hong Z, Arndt J, Li M, Zhi M, Yang F, Wu N (2012) Visible light photocatalytic activity of nitrogen-doped $La_2Ti_2O_7$ nanosheets originating from band gap narrowing. Nano Res 5(3):213–221
17. Wu S, Fang J, Xu X, Liu Z, Zhu X, Xu W (2012) Microemulsion synthesis, characterization of highly visible light responsive rare earth-doped Bi_2O_3. Photochem Photobiol 88:1205–1210
18. Cushing SK, Li J, Meng F, Senty TR, Suri S, Zhi M, Li M, Bristow AD, Wu N (2012) Photocatalytic activity enhanced by plasmonic resonant energy transfer from metal to semiconductor. J Am Chem Soc 134:15033–15041
19. Esquivel K, García-Jimenez MG, Rodríguez FJ, Vega M, Escobar-Alarcón L, Ortiz-Frade L, Godínez LA (2011) Titanium dioxide doped with transition metals ($M_xTi_{1-x}O_2$, M: Ni, Co): synthesis and characterization for its future application as photoanode. J Nanopart Res 13:3313–3325
20. Manriquez J, Godínez LA (2007) Tunning the structural electrical and optical properties of Ti(III)-doped nanocrystalline TiO2 films by electrophoretic deposition time. Thin Solid Films 515: 3402–3413
21. Ramírez J, Godínez LA, Méndez M, Meas Y, Rodríguez F (2010) Heterogeneous photo-electro-Fenton process using different iron supporting materials. J Appl Electrochem 40:1729–1736
22. Fernandez J, Bandara J, López A, Buffat P, Kiwi J (1999) Photoassisted Fenton degradation of nonbiodegradable azo dye (Orange II) in Fe-free solutions mediated by cation transfer membranes. Langmuir 15:185–192
23. Brillas E, Baños MÁ, Garrido JA (2003) Mineralization of herbicide 3,6-dichloro-2-methoxybenzoic acid in aqueous medium by anodic oxidation, electro-Fenton and photoelectro-Fenton. Electrochim Acta 48:1697–1705
24. Daneshvar N, Rasoulifard MH, Khataee AR, Hosseinzadeh F (2007) Removal of C.I. acid orange 7 from aqueous solution by UV irradiation in the presence of ZnO nano-powder. J Hazard Mater 143:95–101
25. Bandala ER, Peláez MA, Dionysiou DD, Gelover S, Garcia J, Macías D (2007) Degradation of 2,4-dichlorophenoxyacetic acid (2,4-D) using cobalt-peroxymonosulfate in Fenton-like process. J Photochem Photobiol A 186:357–363
26. Bandara J, Morrison C, Kiwi J, Pulgarin C, Peringer P (1996) Degradation/decoloration of concentrated solutions of Orange II. kinetics and quantum yield for sunlight induced reactions via Fenton type reagents. J Photochem Photobiol A 99:57–66
27. Kiril Mert B, Yonar T, Yalili Kiliç M, Kestioglu K (2009) Pretreatment studies on olive oil mill effluent using physicochemical, Fenton and Fenton-like oxidations processes. J Hazard Mater 174:122–128